energies

MDPI

Article

Insight into the Thermodynamic Properties of Promising Energetic HNTO·AN Co-Crystal: Heat Capacity, Combustion Energy, and Formation Enthalpy

Amir Abdelaziz [1,*], Ahmed Fouzi Tarchoun [2], Hani Boukeciat [1] and Djalal Trache [1,*]

[1] Energetic Materials Laboratory (EMLab), Teaching and Research Unit of Energetic Processes, Ecole Militaire Polytechnique, BP 17 Bordj El-Bahri, Algiers 16046, Algeria
[2] Energetic Propulsion Laboratory, Teaching and Research Unit of Energetic Processes, Ecole Militaire Polytechnique, BP 17 Bordj El-Bahri, Algiers 16046, Algeria
* Correspondence: amir.abdelaziz920@gmail.com (A.A.); djalaltrache@gmail.com (D.T.)

Abstract: A novel energetic co-crystal composed of hydrazinium 3-nitro-1,2,4-triazol-5-one (HNTO) and ammonium nitrate (AN), as a composite solid propellant oxidizer, was recently developed to substitute either pure ammonium perchlorate (AP) or nitrate. Unfortunately, the thermodynamic properties of this co-crystal or even the pure HNTO are not available in the open literature. Therefore, in this work, the low-temperature heat capacities of HNTO and HNTO·AN co-crystal were measured in the temperature range from 213.15 K to 378.15 K using differential scanning calorimetry. By fitting the heat capacity data, the thermodynamic functions $\Delta H_{298\cdot15K}$, $\Delta G_{298\cdot15K}$, and $\Delta S_{298\cdot15K}$ were derived. In addition, the standard molar energies of combustion $\Delta_c U^\circ$ of HNTO and HNTO·AN co-crystal were determined, and from the combustion results, the standard molar enthalpies of combustion $\Delta_c H^o_m$ and formation $\Delta_f H^o_m$ of these energetic compounds were derived at T = 298.15 K. The set of thermochemical data has been proposed in this work for the first time and will be undoubtedly indispensable information for the development of energetic materials based on HNTO and HNTO·AN co-crystal.

Keywords: ammonium nitrate (AN); hydrazinium 3-nitro-1,2,4-triazol-5-one (HNTO); HNTO·AN co-crystal; calorimetry; heat capacity; combustion; enthalpy of formation

Citation: Abdelaziz, A.; Tarchoun, A.F.; Boukeciat, H.; Trache, D. Insight into the Thermodynamic Properties of Promising Energetic HNTO·AN Co-Crystal: Heat Capacity, Combustion Energy, and Formation Enthalpy. *Energies* **2022**, *15*, 6722. https://doi.org/10.3390/en15186722

Academic Editor: Léo Courty

Received: 30 August 2022
Accepted: 11 September 2022
Published: 14 September 2022

1. Introduction

Energetic materials (EMs) are defined as a class of chemical compounds that store an important extent of energy within their molecular structures, which can be released under some stimuli, such as impact, shock, or a thermal effect [1–6]. The research domain of EMs is still fertile, and its community is continuously looking for novel materials with improved performances. The main concern with EMs is the ability to obtain a satisfactory balance between thermal stability, sensitivity, density, oxygen balance (OB), and combustion/detonation parameters [7,8]. However, the synthesis of novel energetic molecules that encompasses the latter metrics is relatively complex [9]. The scientific community has therefore developed alternative strategies for the design of optimized EMs that are able to fulfill the previous criteria [10–14].

Among these numerous and promising alternatives, the co-crystallization process is an advanced methodology of crystal engineering that permits ordering and combining multiple molecules, among which at least one molecule is energetic, through weak interactions (hydrogen bonds, π-π stacking, and van der Waals forces), without affecting the molecular structure of the co-formers [15,16]. The co-crystallization process allows obtaining novel EMs with adjustable features, such as sensitivity, thermal stability, OB, and density, by just a correct selection of the energetic co-formers [17–19].

The ongoing development of EMs introduced the design of novel energetic co-crystals with promising performance, employing nitrogen-rich molecules, such as ethylene dinitramine (EDNA) [20], 5,5′-dinitro-2H,2H′-3,3′-bi1,2,4-triazole (DNBT) [21], 3,6-dinitropyrazolo[4,3-c]pyrazole [22], etc. Among these emergent nitrogen-rich molecules, hydrazine 3-nitro-1,2,4-triazol-5-one (HNTO) is an energetic salt that has recently been developed and acquires very attractive features, such as high-density ρ = 1.82 g·cm^{-3}, good thermal stability, low sensitivity, and a higher energy content [23–25]. However, this compound suffers from a fairly low OB (−38%). For that reason, a recent study from our research group [26,27] has been conducted in order to overcome the latter issue by combining HNTO with an energetic oxidizer, namely, ammonium nitrate using a co-crystallization process, and thus increasing the overall oxygen balance of the co-crystal. The choice of AN as a co-former to HNTO has been motivated by its highly positive OB (20%), green decomposition products (chlorine-free), and low manufacturing cost [28]. In addition, the co-crystallization of HNTO with AN helped in eliminating the major disadvantage of AN, namely, the polymorphic transition (Phase IV to Phase III) that occurs near room temperature 32 °C [29], which can cause a volume change in AN-based energetic formulations, resulting in damaging and cracking accompanied by a degradation in the mechanical strength [30]. On the other hand, although AP is considered the workhorse oxidizer and the principal choice in composite solid propellants, it displays many drawbacks and hence requires its substitution with environmentally friendly and effective substances for the next generation of solid propellants [31,32].

Despite HNTO·AN co-crystal possessing very interesting energetic properties for application in energetic formulations, it has not been widely acknowledged and the publications reporting such compound are very scarce. In particular, no available thermodynamic properties have been reported for either HNTO·AN co-crystal or pure HNTO in the existing literature. Therefore, the aim of the present study is focused on the determination of the formation enthalpies and the heat capacities of HNTO and HNTO·AN co-crystal through calorimetric measurements. The latter missing or inadequate thermodynamic information will unfortunately limit the uses of HNTO and HNTO·AN and will create a research gap for a better understanding of the structure–property relationship of these energetic compounds that constitute important key parameters in order to help predict their physical properties, such as enthalpies of formation in the gas state [33–35], lattice energies [36], intermolecular forces [37,38], energetic combustion and detonation performances [39,40]. Finally, the newly presented thermodynamic data in the present study will undoubtedly offer indispensable resources for the development of novel propellant formulations, with optimized performances based on HNTO and HNTO·AN as oxidizers.

2. Experimental Section

2.1. Materials and Cocrystal Preparation

AN, with a purity of greater than 99.9%, was purchased from VWR-Prolabo. HNTO was synthesized in our laboratory using a solution of hydrazine hydrate and a solution of 3-nitro-2,4-dihydro-3H-1,2,4-triazol-5-one (NTO) according to the procedure reported elsewhere [26]. The co-crystal of HNTO·AN (see Figure 1) at a molar ratio of 1:3 was prepared through a solvent (methanol) evaporation method for which the details can be found in our previous publication [26,27].

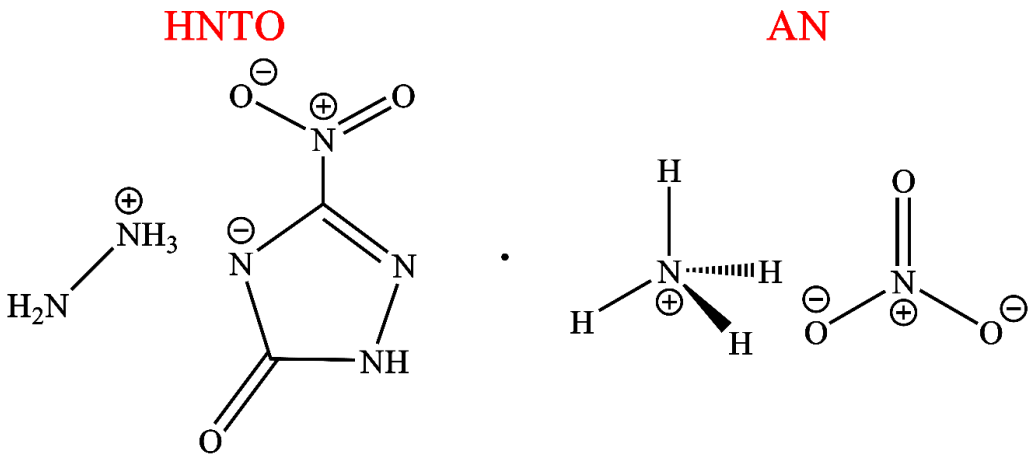

Figure 1. Molecular structure of HNTO (**left**) and AN (**right**).

Before being able to use such compounds for further measurements, they were initially subjected to vacuum evaporation at 333 K and 10^{-2} mbar for more than 24 h to reduce possible traces of solvents and moisture.

2.2. Apparatus and Methods

2.2.1. Heat Capacity Measurements

Conventional differential scanning calorimetry (DSC, PYRIS, PerkinElmer, Waltham, MA, USA) was used to measure the specific heat capacity of the HNTO and the HNTO·AN cocrystal in the solid state. Samples of 2–3 mg, placed in aluminum crucibles, were heated from −70 °C to 120 °C at a heating rate of 10 K·min^{-1} and then cooled at the same heating rate. Each measurement was repeated twice. Heat capacity and temperature calibrations were carried out with sapphire and indium, respectively, using the same experimental conditions [41]. Both sample and sapphire heat capacities were corrected for the empty pan contribution.

2.2.2. Heat of Combustion Determination

The thermochemical measurements were performed on an isoperibol oxygen bomb calorimeter Parr 6200, by Parr Instrument Company, Moline, IL, USA. The samples were placed in a crucible and ignited with a cotton thread on a platinum wire (0.05 mm in diameter and of 99.99% purity) strained between the electrodes.

The energy equivalent of the calorimeter ε_{calor} was determined with a standard reference sample of benzoic acid (BA), according to the recommended procedure of Parr instrument. A series of 10 standardization tests have been carried out and all the obtained values were compared to the NIST [42], Standard Reference Material®39j 26434 ± 3 J·g^{-1} (6317.8778 ± 0.7165 cal·g^{-1}) measured at 298.15 K. As the molecules investigated in this work contain a high nitrogen content, the released N_2 is expected to react with water to form nitric acid [42]. Thus, correction for nitric acid formation has been performed via titration with 0.1 M sodium hydroxide, which leads to a corrected $\Delta_c U_{corr}$ using Equation (1):

$$\Delta U_{corr} = \Delta U - (\Delta_f H^o_{HNO_3} \cdot V_{NaOH} \cdot c_{NaOH}) \quad (1)$$

The atomic weights used were those recommended by the IUPAC Commission.

3. Results and Discussion

3.1. The Specific Heat Capacity and Thermodynamic Function of HNTO and HNTO·AN Cocrystal

The temperature-dependent heat capacities of HNTO and HNTO·AN cocrystal samples are determined from the measured DSC heat flow rate, using a symmetry line correction to account for the heat losses that occur during the heating and cooling scans. For this

correction, it is assumed that the heat losses are only temperature dependent [43]. The heat capacity of pure AN has been previously measured using adiabatic calorimetry and reported in the literature [44]. The resulting heat capacities of HNTO and HNTO·AN cocrystal together with the heat capacity of AN taken from [44] are shown in Figure 2.

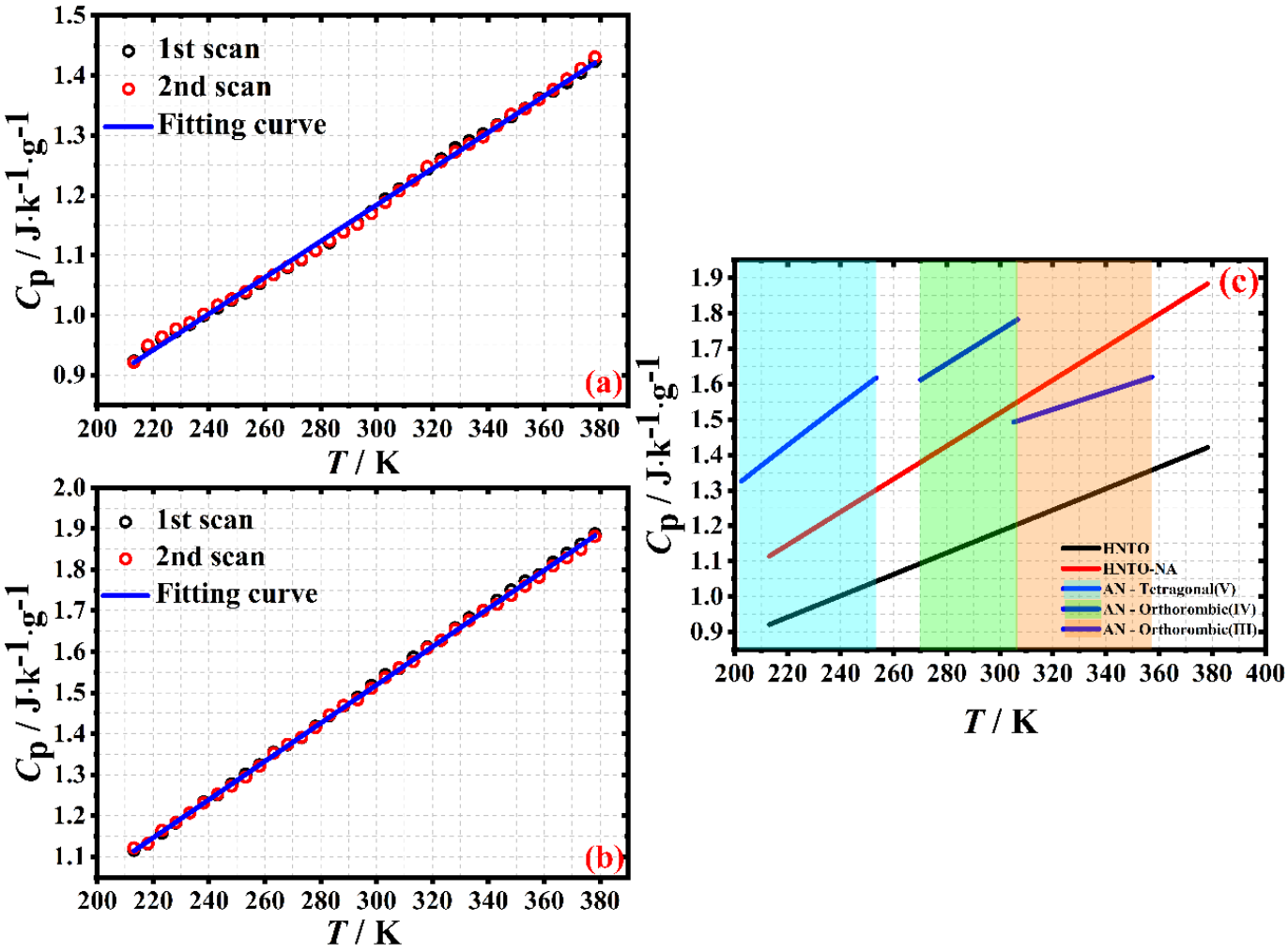

Figure 2. (**a**) Plot of the experimental and fitted heat capacities of HNTO as a function of temperature. (**b**) Plot of the experimental and fitted heat capacities of HNTO·AN cocrystal as a function of temperature. (**c**) Comparison between the fitted heat capacities of AN from [44], HNTO, and HNTO·AN cocrystal.

It can be seen from Figure 2a,b that the solid-state specific heat capacity C_p(cr) of HNTO and HNTO·AN cocrystal shows a smooth increase with the temperature from 213.15 K to 378.15 K. On the other hand, the pure AN observes an abrupt change in its heat capacity when heating from 213.15 K to 378.15 K, and such an apparent discontinuity is due to the solid–solid transition of AN that undergoes two visible transitions from tetragonal (V) to orthorhombic (IV) crystal structure at T = 255 K and a subsequent transition from orthorhombic (IV) to orthorhombic (III) structure at T = 305 K [29,44].

It is possible to denote that even though AN observes solid–solid transitions, the HNTO·AN cocrystal is stable and does not display any shift in the heat capacity and no thermal anomalies could be observed in the entire experimental temperature range. Thus, the latter finding highlights the aptitude of the co-crystallization process of AN with HNTO to suppress the latter solid–solid transition, hence stabilizing the AN crystal structure. This phase-stabilized ammonium nitrate (PSAN) exhibits a very interesting behavior since PSAN

overcomes the major drawbacks of AN by avoiding the volume change (approximately 3.8% volume change) and density change caused by the solid–solid transition of AN at a low temperature of 32 °C that induces a porous structure and poor mechanical strength [30]. In addition, it is possible to denote that the heat capacity of the solid cocrystal is found to be higher than that of HNTO within the entire studied temperature range (see Figure 2c). However, the heat capacity of the cocrystal is lower than pure AN heat capacity when the crystalline phase of AN is tetragonal (V) and orthorhombic (IV), while it becomes higher when the crystalline phase of AN shifts to orthorhombic (III) at approximately T = 305K (see Figure 2c).

To further evaluate the thermodynamic functions of pure HNTO and HNTO·AN co-crystal samples, their experimental specific heat capacities measured with the two DSC runs were fitted using a linear model of two parameters α and β within a temperature range temperature from 213.15 K to 378.15 K as follow:

$$C_p(T)\ /\mathrm{J}\cdot\mathrm{g}^{-1}\cdot\mathrm{K}^{-1} = \alpha\ (T\ /\ K)+\beta \quad (2)$$

The fitting parameters α and β, the regression coefficients r^2 with the relative mean square error (*RMSE*) of the linear fitting curves and the heat capacity for HNTO and HNTO·AN at 298.15 K are summarized in Table 1.

Table 1. Fitting parameters α and β, regression coefficients r^2 of the linear fitting curves, and the heat capacity for HNTO and HNTO·AN cocrystal at 298.15 K.

Compound	Fitting Parameters		C_p (cr, 298.15 K)/J·g^{-1}·K^{-1}	r^2	*RMSE*
HNTO	α	0.27562 ± 0.00468	1.1790 ± 0.0093	0.9982	0.00623
	β	0.00303 ± 1.56263 × 10^{-5}			
HNTO·AN	α	0.12112 ± 0.00353	1.5105 ± 0.0070	0.9996	0.00469
	β	0.00466 ± 1.17659 × 10^{-5}			

It can be noticed from Table 1 that the fitting C_p(T) curves represent a good linear approximation over the studied experimental temperature range with r^2 values exceeding 0.99. In addition, the evaluated RMSE (see Table 1) of the fitting curves is clearly within the uncertainties of the calorimetric measurements (±3%) which supports the fact that the linear fitting can properly simulate the measured heat capacity data of HNTO and HNTO·AN. Despite the studied experimental temperature range being from 213.15 K to 378.15 K, the fitting C_p function is stable and continuous, thus serving as a benchmark function for the application of HNTO and HNTO·AN co-crystal within this temperature range.

By exploiting the heat capacity data (see Figure 2 and Table 1), the thermodynamic functions of the enthalpy change, the entropy change, and the Gibbs free energy change of HNTO and HNTO·AN were evaluated within 213.15 K to 378.15 K using Equations (3)–(5) by taking T_0 = 298.15 K as a reference temperature and the results are listed in Table 2. Obviously, the values of $H_T-H_{T_0}$, $S_T-S_{T_0}$, and $G_T-G_{T_0}$, present an increasing trend within the studied experimental temperature range. In addition, the values of $H_T-H_{T_0}$, $S_T-S_{T_0}$, and $G_T-G_{T_0}$ are all negative when the temperature is below 298.15 K and change sign above 298.15 K.

$$H_T-H_{T_0} = \int_{T_0}^{T} C_p\mathrm{d}T \quad (3)$$

$$S_T-S_{T_0} = \int_{T_0}^{T} \frac{C_p}{T}\mathrm{d}T \quad (4)$$

$$G_T-G_{T_0} = \int_{T_0}^{T} C_p\mathrm{d}T - T\int_{T_0}^{T} \frac{C_p}{T}\mathrm{d}T \quad (5)$$

Table 2. The heat capacity C_p, enthalpy change ($H_T - H_{T_0}$), entropy change ($S_T - S_{T_0}$), and Gibbs free energy change ($G_T - G_{T_0}$) data at T_0 = 298.15 K of pure HNTO and HNTO·AN cocrystal.

	HNTO				HNTO·AN			
T / K	C_p / J·g^{-1}·K^{-1}	$\Delta H_{298.15K}$ / J·g^{-1}	$\Delta S_{298.15K}$ / J·g^{-1}·K^{-1}	$\Delta G_{298.15K}$ / J·g^{-1}	C_p / J·g^{-1}·K^{-1}	$\Delta H_{298.15K}$ / J·g^{-1}	$\Delta S_{298.15K}$ / J·g^{-1}·K^{-1}	$\Delta G_{298.15K}$ / J·g^{-1}
213.15	0.9212	−155.1	−0.35	−80.5	1.1149	−212.8	−0.44	−119.7
218.15	0.9363	−147.2	−0.33	−75.5	1.1382	−202.2	−0.41	−112.6
228.15	0.9666	−130.9	−0.29	−65.7	1.1849	−180.2	−0.36	−98.3
238.15	0.9969	−114.0	−0.24	−56.0	1.2315	−157.2	−0.31	−84.1
248.15	1.0272	−96.5	−0.20	−46.4	1.2782	−133.3	−0.26	−70.0
258.15	1.0575	−78.4	−0.16	−36.9	1.3248	−108.5	−0.20	−55.9
268.15	1.0877	−59.7	−0.12	−27.5	1.3714	−82.8	−0.15	−41.9
278.15	1.1180	−40.4	−0.08	−18.3	1.4181	−56.1	−0.10	−27.9
288.15	1.1483	−20.5	−0.04	−9.1	1.4647	−28.5	−0.05	−13.9
298.15	1.1786	0.0	0.00	0.0	1.5114	0.0	0.00	0.0
308.15	1.2089	21.1	0.04	9.0	1.5580	29.5	0.05	13.9
318.15	1.2392	42.9	0.08	17.9	1.6046	59.9	0.10	27.7
328.15	1.2695	65.2	0.12	26.7	1.6513	91.2	0.15	41.5
338.15	1.2998	88.1	0.16	35.4	1.6979	123.5	0.20	55.3
348.15	1.3300	111.7	0.19	44.1	1.7446	156.6	0.25	69.0
358.15	1.3603	135.9	0.23	52.6	1.7912	190.8	0.30	82.7
368.15	1.3906	160.6	0.27	61.1	1.8378	225.8	0.35	96.3
378.15	1.4209	186.0	0.31	69.5	1.8845	261.8	0.40	110.0

3.2. The Standard Molar Enthalpies of Formation of HNTO and HNTO·AN

The enthalpy of formation $\Delta_f H_m^o(\mathrm{cr})$ of HNTO and HNTO·AN derived from combustion experiments are referred to as the crystalline state of the two compounds at a reference temperature T = 298.15 K. The values of the standard molar combustion energies $\Delta_c U_m^o(\mathrm{cr})$ correspond to the idealized combustion reactions of the solid energetic crystals.

For HNTO, the idealized combustion reaction is represented by the following equation:

$$\mathbf{C_2H_6O_3N_{6(s)} + 2O_{2(g)} \rightarrow 2CO_{2(g)} + 3H_2O_{(l)} + 3N_{2(g)}} \quad (6)$$

The specific combustion energy measured for HNTO is found to be -8716.6 ± 6.1 J·g^{-1} after correction from the nitric acid contribution (see Section 2.2), and the reported value is the average of three separate measurements. Using the experimental energy of combustion of HNTO, the standard specific enthalpy of combustion of HNTO can be calculated through the following equations:

$$\mathbf{\Delta_c H = \Delta_c U + \Delta n_g RT} \quad (7)$$

$$\mathbf{\Delta_c H_m^o = \sum \Delta_f H_m^o(products) - \sum \Delta_f H_m^o(reactants)} \quad (8)$$

Thus, by applying Hess thermodynamical cycle to the idealized combustion reaction of HNTO, it was possible to compute the standard molar enthalpy of formation of HNTO at 298.15 K. By considering the heat of formation of the combustion products (carbon dioxide $\Delta_f H_m^o(CO_2, g) = (-393.5 \pm 0.13)$ kJ·mol^{-1} [33] and water $\Delta_f H_m^o(H_2O, l) = (-285.83 \pm 0.04)$ kJ·mol^{-1} [33], the formation enthalpy of HNTO, $\Delta_f H_m^o(\mathrm{HNTO, cr}) = (-231.4 \pm 1.4)$ kJ·mol^{-1} was obtained. Despite the high nitrogen content in the molecular structure of HNTO, the obtained negative heat of formation of this compound demonstrates an exothermic contribution during its formation, indicating the non-negligible chemical stability of HNTO.

An analogous strategy is therefore applied to calculate the heat of formation of HNTO·AN co-crystal using the bomb calorimeter. For that reason, it is necessary to determine the equilibrium composition of the combustion reaction products of the HNTO·AN co-crystal in order to apply the Hess thermodynamic cycle. The studied HNTO·AN co-crystal is assumed to be a composite explosive formed by the association of an organic

HNTO molecule and an inorganic ammonium nitrate molecule. The HNTO thermal decomposition is assumed ideal (CO_2, H_2O, and N_2 as combustion products) under an excess of oxygen in the bomb calorimeter but on the other hand, the decomposition path of AN can be difficult to assume because of its physical and chemical complexity that leads to many reaction paths [45,46] (see Table 3). Consequently, according to the latter challenges, assuming an ideal combustion reaction of HNTO·AN co-crystal would not be consistent.

Table 3. Single-step decomposition reactions of AN (positive values of heat of reaction indicate endothermic reactions, negative values exothermic). The reaction heat, $\Delta_r h$, is expressed at T = 298.15 K [46]. "Reprinted/adapted with permission from Ref. [46]. 2022, John Wiley".

Rxn N°	Decomposition Reactions	$\Delta_r H^o_m$(AN)/kJ·mol^{-1}
1	$NH_4NO_3 \rightleftarrows HNO_3 + NH_3$	+179.9
2	$NH_4NO_3 \rightarrow N_2O + 2\,H_2O$	−42.3
3	$4\,NH_4NO_3 \rightarrow 3\,N_2 + N_2O_4 + 8\,H_2O$	−121.1
4	$NH_4NO_3 \rightarrow N_2 + 2H_2O + \frac{1}{2}\,O_2$	−123.9
5	$NH_4NO_3 \rightarrow NO + \frac{1}{2}\,N_2 + 2\,H_2O$	−32.6
6	$3\,NH_4NO_3 \rightarrow 2N_2 + N_2O_3 + 6\,H_2O$	−95.0
7	$5\,NH_4NO_3 \rightarrow 2\,HNO_3 + 4\,N_2 + 9\,H_2O$	−129.1
8	$8\,NH_4NO_3 \rightarrow 16\,H_2O + 2\,NO_2 + 4\,NO + 5\,N_2$	−70.0
9	$4\,NH_4NO_3 \rightarrow 3\,N_2 + 2\,NO_2 + 8\,H_2O$	−377.1
10	$4\,NH_4NO_3 \rightarrow 2\,NH_3 + 3\,NO_2 + NO + N_2 + 5\,H_2O$	+82.2

Therefore, we have attempted to realize thermal decomposition tests of AN in the bomb calorimeter, in order to gain a better understanding of its thermal decomposition mechanism in the working experimental conditions of the bomb calorimeter. However, performing an ignition of AN by itself cannot be achieved under an excess of oxygen in the bomb, and the presence of an additional fuel is necessary in order to initiate its decomposition reaction. Thus, the solid AN sample has been mixed with BA powder at different mass ratios for ignition aid purposes. Solid composites consisting of different weight fractions of BA (30 wt.% to 70 wt.%) and ammonium nitrate have been tested in the bomb calorimeter and the reaction energies $\Delta_r U$ have been recorded and their variation with BA weight fraction is presented in Figure 3a.

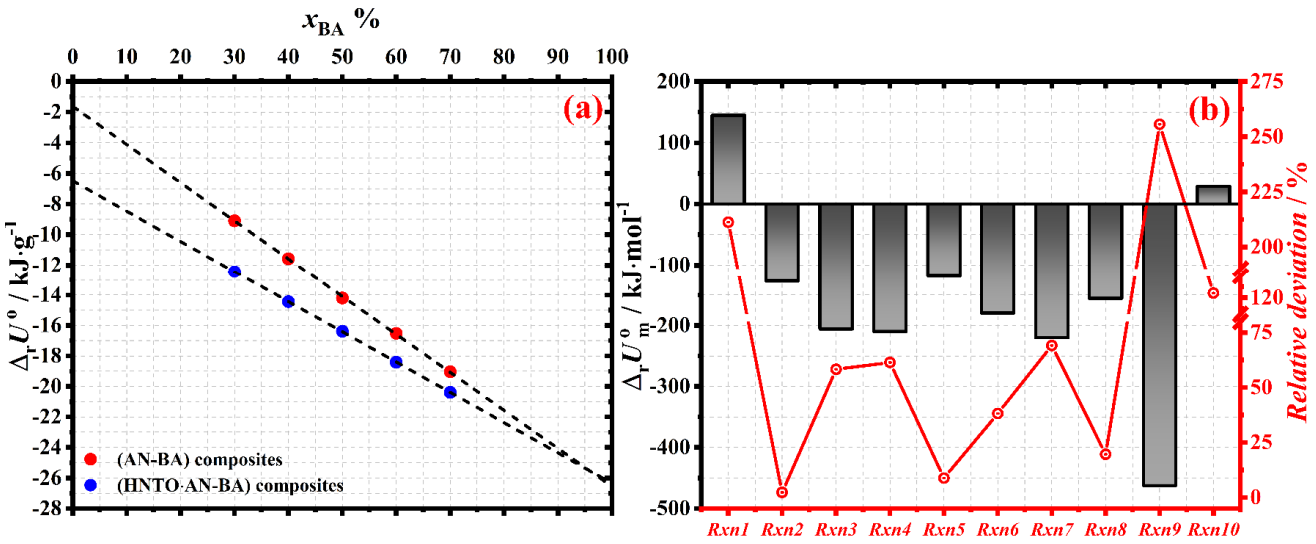

Figure 3. (**a**) The measured combustion energy of BA-AN composites vs. the weight fraction of BA. (**b**) Columns plot of the calculated energies of reaction $\Delta_r U^o_m$ of each reaction path in Table 3 and its relative deviation from the experimental value derived from the bomb calorimetry.

It is possible to denote from Figure 3a, that the variation of the measured reaction energy $\Delta_r U^o$ of the BA-AN composite follow a linear evolution with the BA weight fraction. The fitting parameters **a** and ***b***, the regression coefficients r^2 of the linear fitting curves ($\Delta_r U^o = a x_{BA} + b$) are summarized in Table 4. The regression coefficient value r^2 surpasses 0.999, which indicates that the measured energy is perfectly fitted with a straight line.

Table 4. Linear fitting parameters **a**, **b**, and regression coefficients r^2 of the combustion energy of (AN-BA) and (HNTO·AN-BA) composites vs. the weight fraction of BA.

Compound	Fitting Parameters		r^2
AN-BA	**a**	-0.24933 ± 0.00217	0.9998
	b	-1.62282 ± 0.09694	
HNTO·AN-BA	**a**	$-0.19858 \pm 6.15467 \times 10^{-4}$	0.9999
	b	-6.4836 ± 0.03198	

The decomposition energy of pure AN in the bomb calorimeter could be extracted from Figure 3a by an extrapolation of the linear fitting curve to $x_{BA} = 0$ (absence of BA) and the obtained thermal decomposition energy of AN is found to be $\Delta_r U^o_{m,exp}$**(AN)** = (-130 ± 8) kJ·mol^{-1}.

By considering the experimental decomposition energy of AN measured previously, it becomes possible to compare it to the energy $\Delta_r U^o_m$**(AN)** released from the decomposition reaction of the AN, according to the multiple reaction pathways presented in Table 3. The values of the decomposition energy $\Delta_r U^o_m$**(AN)** (see Figure 3b) were derived from the heat of the reaction $\Delta_r H^o_m$**(AN)** data shown in Table 3, and their deviation from the measured experimental value $\Delta_r U^o_{m,exp}$**(AN)** was calculated using Equation (9) for which the results are shown in Figure 3b as well.

$$\textit{relative deviation} / \% = 100 \cdot \left| \frac{\Delta_r U^o_m(\mathbf{AN}) - \Delta_r U^o_{m,exp}(\mathbf{AN})}{\Delta_r U^o_{m,exp}(\mathbf{AN})} \right| \quad (9)$$

The minimal deviation of $\Delta_r U^o_m$**(AN)** (calculated from Table 3) from the experimental decomposition energy $\Delta_r U^o_{m,exp}$**(AN)** measured by the calorimeter has been reached by the reaction path N° 2 (see Figure 3b), which was presented in Table 3 by the following reaction:

$$\mathbf{NH_4NH_3 \rightarrow N_2O + 2H_2O} \quad (10)$$

Therefore, taking into account the decomposition pathways of the AN determined previously, it could be possible to adopt a certain decomposition pathway for the HNTO·AN (1:3) co-crystal as follows:

$$\begin{cases} \mathbf{C_2H_6O_3N_{6(s)} + 2O_{2(g)} \rightarrow 2CO_{2(g)} + 3H_2O_{(l)} + 3N_{2(g)}} \\ \mathbf{NH_4NO_{3(s)} \rightarrow N_2O_{(g)} + 2H_2O_{(l)}} \end{cases} \quad (11)$$

$$\mathbf{[C_2H_6O_3N_6 + 3NH_4NO_3]_{(s)} + 2O_{2(g)} \rightarrow 3N_2O_{(g)} + 2CO_{2(g)} + 9H_2O_{(l)} + 3N_{2(g)}} \quad (12)$$

Thus, using the Hess thermodynamical cycle, it is possible to determine the formation enthalpy of the co-crystal using the reaction path of Equations (11) and (12) and the combustion energy of the co-crystal that was measured by the bomb calorimeter. However, the combustion test performed in the calorimeter showed that the HNTO·AN co-crystal observed an incomplete ignition because of the presence of AN, as explained above, which required the use of the BA as a combustion aid additive. Therefore, a similar methodology to that used to determine the decomposition energy of AN has been employed in order to obtain the energy of combustion of the HNTO·AN co-crystal. The combustion of solid composites consisting of varying weight fractions of benzoic acid (30 wt.% to 70 wt.%) and HNTO·AN co-crystal has been performed in the bomb calorimeter and the combustion energy $\Delta_c U$ has been accordingly recorded and its variation with the benzoic acid weight fraction is plotted in Figure 2a.

Comparable to the AN-BA composite, the combustion energy of the HNTO·AN-BA composite also exhibits a strong linear evolution with the weight fraction of the benzoic acid. A linear fitting of the experimental combustion energy $\Delta_c U$ data has been performed and the fitting parameters are summarized in Table 4. Thus, an extrapolation of the linear fitting curve to $x_{BA} = 0$ (absence of BA) permits to obtain the combustion energy of the HNTO·AN co-crystal $\Delta_c U^o_{m,exp}$**(HNTO·AN)** = (-2608 ± 13) kJ·mol^{-1}.

Thereby, we calculated the molar formation enthalpy of the HNTO·AN co-crystal at 298.15 K, considering the heat of formation of the combustion products (carbon dioxide $\Delta_f H^o_m(CO_2, g) = (-393.5 \pm 0.13)$ kJ·mol^{-1}, water $\Delta_f H^o_m(H_2O, l) = (-285.83 \pm 0.04)$ kJ·mol^{-1}, and nitrous oxide $\Delta_f H^o_m(N_2O, g) = 82.05$ kJ·mol^{-1} [47], and the obtained molar formation enthalpy of HNTO·AN corresponds to $\Delta_f H^o_m(\text{HNTO·AN, cr}) = (-505 \pm 13)$ kJ·mol^{-1}. The approach for estimating the thermodynamic molar formation enthalpy of HNTO·AN co-crystal used in this study is dependent on the assumption that the thermal decomposition of AN follows just a single reaction mechanism and that this reaction pathway is not influenced by the co-crystallization process and remains unchanged during the decomposition of the co-crystal.

It is worth mentioning that the formation enthalpy of the HNTO·AN co-crystal is quite different from that of the solid mixture (calculated as $x_{AN}\Delta_f H^o_m$**(AN,cr)**$+x_{HNTO}\Delta_f H^o_m$**(HNTO,cr)**), which highlights the difference between the co-crystal and the solid mixture. In addition, the obtained formation enthalpy of the HNTO·AN co-crystal is found to be lower than that of its co-formers $\Delta_f H^o_m$**(AN,cr)=** -365.6 kJ·mol^{-1} [46], $\Delta_f H^o_m$**(HNTO,cr)** = **(-231.4 ± 1.4) kJ·mol^{-1}**, revealing that the obtained co-crystal is chemically more stable than its co-formers.

4. Conclusions

In the present study, the heat capacities of energetic HNTO and its co-crystal HNTO·AN were measured using differential scanning calorimetry. The heat capacity equations of the two energetic compounds are found to be $C_p(T)/\text{J·g}^{-1}\text{·K}^{-1}$ = 0.27562 (T/K)+0.00303 and $C_p(T)$ /J·g^{-1}·K^{-1} = 0.12112 (T/K)+0.00466 for HNTO and HNTO·AN co-crystal, respectively, within a temperature range of 213.15 K to 378.15 K. Based on the heat capacity data, the enthalpy change, the entropy change and the Gibbs energy change of HNTO and HNTO·AN are also determined, taking 298.15 K as the benchmark temperature. The measurements of the combustion energies of HNTO and HNTO·AN cocrystal in conjunction with the application of the Hess thermodynamic cycle enable their heats of formation to be determined. The thermodynamic results obtained can provide valuable information for further thermochemical calculations involving these energetic materials. All the obtained results will certainly be utilized as input parameters for the prediction of the detonation and combustion parameters of HNTO and HNTO·AN and will also help to design future propellant formulations with optimized performances based on these two nitrogen-rich oxidizers.

Author Contributions: A.A.: Conceptualization, methodology, resources, investigation, data treatment, writing—original draft. A.F.T. and H.B.: Review and editing of the manuscript draft. D.T.: Supervision, conceptualization, review and editing. All authors have read and agreed to the published version of the manuscript.

Funding: The authors do not have any funding or financial support to declare.

Conflicts of Interest: The authors declare no competing financial and/or other interests that might be perceived to influence the results and/or discussion reported in this paper.

References

1. Herweyer, D.; Brusso, J.L.; Murugesu, M. Modern trends in "Green" primary energetic materials. *New J. Chem.* **2021**, *45*, 10150–10159. [CrossRef]
2. Tariq, Q.; Manzoor, S.; Cao, W.; Dong, W.; Arshad, F.; Zhang, J. Synthesis and Energetic Properties of Trending Metal-Free Potential Green Primary Explosives: A Review. *ChemistrySelect* **2022**, *7*, e202200017. [CrossRef]

3. Huang, B.; Xue, Z.; Fu, X.; Yan, Q.-L. Advanced crystalline energetic materials modified by coating/intercalation techniques. *Chem. Eng. J.* **2020**, *417*, 128044. [CrossRef]
4. Pang, W.; Deng, C.; Li, H.; DeLuca, L.T.; Ouyang, D.; Xu, H.; Fan, X. Effect of Nano-Sized Energetic Materials (nEMs) on the Performance of Solid Propellants: A Review. *Nanomaterials* **2021**, *12*, 133. [CrossRef]
5. Klapötke, T.M. *Chemistry of High-Energy Materials*, 4th ed.; de Gruyter: Berlin, Germany, 2022; p. 369.
6. Trache, D.; Klapötke, T.M.; Maiz, L.; Abd-Elghany, M.; DeLuca, L.T. Recent advances in new oxidizers for solid rocket propulsion. *Green Chem.* **2017**, *19*, 4711–4736. [CrossRef]
7. Anniyappan, M.; Talawar, M.B.; Sinha, R.K.; Murthy, K.P.S. Review on Advanced Energetic Materials for Insensitive Munition Formulations. *Combust. Explos. Shock Waves* **2020**, *56*, 495–519. [CrossRef]
8. Ma, Q.; Zhang, Z.; Yang, W.; Li, W.; Ju, J.; Fan, G. Strategies for constructing melt-castable energetic materials: A critical review. *Energetic Mater. Front.* **2021**, *2*, 69–85. [CrossRef]
9. Muravyev, N.V.; Meerov, D.B.; Monogarov, K.A.; Melnikov, I.N.; Kosareva, E.K.; Fershtat, L.L.; Sheremetev, A.B.; Dalinger, I.L.; Fomenkov, I.V.; Pivkina, A.N. Sensitivity of energetic materials: Evidence of thermodynamic factor on a large array of CHNOFCl compounds. *Chem. Eng. J.* **2021**, *421*, 129804. [CrossRef]
10. Zhang, X.; Pan, L.; Wang, L.; Zou, J.-J. Review on synthesis and properties of high-energy-density liquid fuels: Hydrocarbons, nanofluids and energetic ionic liquids. *Chem. Eng. Sci.* **2018**, *180*, 95–125. [CrossRef]
11. Zhang, Q.; Shreeve, J.n.M. Energetic ionic liquids as explosives and propellant fuels: A new journey of ionic liquid chemistry. *Chem. Rev.* **2014**, *114*, 10527–10574. [CrossRef]
12. Yan, Q.-L.; Zhao, F.-Q.; Kuo, K.K.; Zhang, X.-H.; Zeman, S.; DeLuca, L.T. Catalytic effects of nano additives on decomposition and combustion of RDX-, HMX-, and AP-based energetic compositions. *Prog. Energy Combust. Sci.* **2016**, *57*, 75–136. [CrossRef]
13. Gruhne, M.S.; Lommel, M.; Wurzenberger, M.H.H.; Klapötke, T.M.; Stierstorfer, J. Investigation of Ethylenedinitramine as a Versatile Building Block in Energetic Salts, Cocrystals, and Coordination Compounds. *Inorg. Chem.* **2021**, *60*, 4816–4828. [CrossRef] [PubMed]
14. Kuchurov, I.V.; Zharkov, M.N.; Fershtat, L.L.; Makhova, N.; Zlotin, S.G. Prospective Symbiosis of Green Chemistry and Energetic Materials. *ChemSusChem* **2017**, *10*, 3914–3946. [CrossRef]
15. Thayyil, A.R.; Juturu, T.; Nayak, S.; Kamath, S. Pharmaceutical Co-Crystallization: Regulatory Aspects, Design, Characterization, and Applications. *Adv. Pharm. Bull.* **2020**, *10*, 203–212. [CrossRef] [PubMed]
16. Chaudhari, S.; Nikam, S.A.; Khatri, N.; Wakde, S. Co-Crystals: A Review. *J. Drug Deliv. Ther.* **2018**, *8*, 350–358. [CrossRef]
17. Pang, W.-Q.; Wang, K.; Zhang, W.; Luca, L.; Fan, X.-Z.; Li, J.-Q. CL-20-Based Cocrystal Energetic Materials: Simulation, Preparation and Performance. *Molecules* **2020**, *25*, 4311. [CrossRef]
18. Sultan, M.; Wu, J.; Haq, I.U.; Imran, M.; Yang, L.; Wu, J.; Lu, J.; Chen, L. Recent Progress on Synthesis, Characterization, and Performance of Energetic Cocrystals: A Review. *Molecules* **2022**, *27*, 4775. [CrossRef]
19. Xue, Z.-H.; Zhang, X.-X.; Huang, B.; Cheng, J.; Wang, K.; Yang, Z.; Yan, Q.-L. Assembling of Hybrid Nano-sized HMX/ANPyO Cocrystals Intercalated with 2D High Nitrogen Materials. *Cryst. Growth Des.* **2021**, *21*, 4488–4499. [CrossRef]
20. Aakeröy, C.B.; Wijethunga, T.K.; Desper, J. Crystal Engineering of Energetic Materials: Co-crystals of Ethylenedinitramine (EDNA) with Modified Performance and Improved Chemical Stability. *Chem. A Eur. J.* **2015**, *21*, 11029–11037. [CrossRef]
21. Bennion, J.C.; McBain, A.; Son, S.F.; Matzger, A.J. Design and Synthesis of a Series of Nitrogen-Rich Energetic Cocrystals of 5,5′-Dinitro-2*H*,2*H*′-3,3′-bi-1,2,4-triazole (DNBT). *Cryst. Growth Des.* **2015**, *15*, 2545–2549. [CrossRef]
22. Zhang, J.; Parrish, D.A.; Jean'ne, M.S. Curious cases of 3, 6-dinitropyrazolo [4, 3-c] pyrazole-based energetic cocrystals with high nitrogen content: An alternative to salt formation. *Chem. Commun.* **2015**, *51*, 7337–7340. [CrossRef] [PubMed]
23. Zhang, M.; Li, C.; Gao, H.; Fu, W.; Li, Y.; Tang, L.; Zhou, Z. Promising hydrazinium 3-Nitro-1,2,4-triazol-5-one and its analogs. *J. Mater. Sci.* **2016**, *51*, 10849–10862. [CrossRef]
24. Yi, J.-H.; Zhao, F.-Q.; Gao, H.-X.; Xu, S.-Y.; Wang, M.-C.; Hu, R.-Z. Preparation, characterization, non-isothermal reaction kinetics, thermodynamic properties, and safety performances of high nitrogen compound: Hydrazine 3-nitro-1,2,4-triazol-5-one complex. *J. Hazard. Mater.* **2008**, *153*, 261–268. [CrossRef] [PubMed]
25. Yi, J.-H.; Zhao, F.-Q.; Ren, Y.-H.; Xu, S.-Y.; Ma, H.-X.; Hu, R.-Z. Thermal decomposition mechanism and quantum chemical investigation of hydrazine 3-nitro-1,2,4-triazol-5-one (HNTO). *J. Therm. Anal.* **2009**, *100*, 623–627. [CrossRef]
26. Hanafi, S.; Trache, D.; Meziani, R.; Boukciat, H.; Mezroua, A.; Tarchoun, A.F.; Derradji, M. Synthesis, characterization and thermal decomposition behavior of a novel HNTO/AN co-crystal as a promising rocket propellant oxidizer. *Chem. Eng. J.* **2020**, *417*, 128010. [CrossRef]
27. Hanafi, S.; Trache, D.; Mezroua, A.; Boukeciat, H.; Meziani, R.; Tarchoun, A.F.; Abdelaziz, A. Optimized energetic HNTO/AN co-crystal and its thermal decomposition kinetics in the presence of energetic coordination nanomaterials based on functionalized graphene oxide and cobalt. *RSC Adv.* **2021**, *11*, 35287–35299. [CrossRef]
28. Jos, J.; Mathew, S. Ammonium Nitrate as an Eco–Friendly Oxidizer for Composite Solid Propellants: Promises and Challenges. *Crit. Rev. Solid State Mater. Sci.* **2016**, *42*, 470–498. [CrossRef]
29. Wu, H.B.; Nin Chan, M.; Chan, C.K. FTIR Characterization of Polymorphic Transformation of Ammonium Nitrate. *Aerosol Sci. Technol.* **2007**, *41*, 581–588. [CrossRef]

30. Lee, T.; Chen, J.W.; Lee, H.L.; Lin, T.Y.; Tsai, Y.C.; Cheng, S.-L.; Lee, S.-W.; Hu, J.-C.; Chen, L.-T. Stabilization and spheroidization of ammonium nitrate: Co-crystallization with crown ethers and spherical crystallization by solvent screening. *Chem. Eng. J.* **2013**, *225*, 809–817. [CrossRef]
31. Hanafi, S.; Trache, D.; Meziani, R.; Boukeciat, H.; Abdelaziz, A.; Tarchoun, A.F.; Mezroua, A. Catalytic reactivity of graphene oxide stabilized Fe complexe of triaminoguanidine on thermolysis of HNTO/AN co-crystal. *Thermochim. Acta* **2022**, *717*. [CrossRef]
32. Hanafi, S.; Trache, D.; Meziani, R.; Boukeciat, H.; Tarchoun, A.F.; Abdelaziz, A.; Mezroua, A. Thermal decomposition and kinetic modeling of HNTO/AN-based composite solid propellant in the presence of GO-based nanocatalyst. *FirePhysChem* **2022**. [CrossRef]
33. Emel'Yanenko, V.N.; Kabo, G.J.; Verevkin, S.P. Measurement and Prediction of Thermochemical Properties: Improved Increments for the Estimation of Enthalpies of Sublimation and Standard Enthalpies of Formation of Alkyl Derivatives of Urea. *J. Chem. Eng. Data* **2006**, *51*, 79–87. [CrossRef]
34. Abdelaziz, A.; Zaitsau, D.H.; Buzyurov, A.V.; Verevkin, S.P.; Schick, C. Sublimation thermodynamics of nucleobases derived from fast scanning calorimetry. *Phys. Chem. Chem. Phys.* **2020**, *22*, 838–853. [CrossRef]
35. Abdelaziz, A.; Zaitsau, D.; Kuratieva, N.; Verevkin, S.; Schick, C. Melting of nucleobases. Getting the cutting edge of "Walden's Rule". *Phys. Chem. Chem. Phys.* **2019**, *21*, 12787–12797. [CrossRef]
36. Ouvrard, C.; Mitchell, J.B. Can we predict lattice energy from molecular structure? *Crystallogr. B. Struct. Sci. Cryst. Eng. Mater.* **2003**, *59*, 676–685. [CrossRef]
37. Siewert, R.; Ludwig, R.; Verevkin, S.P. Non-covalent interactions in molecular systems: Thermodynamic evaluation of the hydrogen bond strength in aminoalcohols. *Phys. Chem. Chem. Phys.* **2021**, *23*, 25226–25238. [CrossRef]
38. Siewert, R.; Zherikova, K.V.; Verevkin, S.P. Non-Covalent Interactions in Molecular Systems: Thermodynamic Evaluation of the Hydrogen-Bond Strength in Amino-Ethers and Amino-Alcohols. *Chem. Eur. J.* **2022**, 28. [CrossRef]
39. Klapötke, T.M.; Witkowski, T.G. Nitrogen-Rich Energetic 1, 2, 5-Oxadiazole-Tetrazole–Based Energetic Materials. *Propellants Explos. Pyrotech.* **2015**, *40*, 366–373. [CrossRef]
40. Klapötke, T.M.; Cudziło, S.; Trzciński, W.A. An Answer to the Question about the Energetic Performance of TKX-50. *Propellants, Explos. Pyrotech.* **2022**, *47*. [CrossRef]
41. Sarge, S.M.; Hemminger, W.; Gmelin, E.; Höhne, G.W.H.; Cammenga, H.K.; Eysel, W. Metrologically based procedures for the temperature, heat and heat flow rate calibration of DSC. *J. Therm. Anal.* **1997**, *49*, 1125–1134. [CrossRef]
42. Mentado-Morales, J.; Hernández-Sánchez, E.; Regalado-Méndez, A.; Peralta-Reyes, E. An isoperibolic combustion calorimeter developed to measure the enthalpy of combustion of organic compounds. *J. Therm. Anal. Calorim.* **2017**, *127*, 2307–2314. [CrossRef]
43. Cebe, P.; Partlow, B.P.; Kaplan, D.L.; Wurm, A.; Zhuravlev, E.; Schick, C. Using flash DSC for determining the liquid state heat capacity of silk fibroin. *Thermochim. Acta* **2015**, *615*, 8–14. [CrossRef]
44. Nagatani, M.; Seiyama, T.; Sakiyama, M.; Suga, H.; Seki, S. Heat Capacities and Thermodynamic Properties of Ammonium Nitrate Crystal: Phase Transitions between Stable and Metastable Phases. *Bull. Chem. Soc. Jpn.* **1967**, *40*, 1833–1844. [CrossRef]
45. Chaturvedi, S.; Dave, P.N. Review on Thermal Decomposition of Ammonium Nitrate. *J. Energetic Mater.* **2013**, *31*, 1–26. [CrossRef]
46. Babrauskas, V.; Leggett, D. Thermal decomposition of ammonium nitrate. *Fire Mater.* **2020**, *44*, 250–268. [CrossRef]
47. Risch, T.K. *Curve Fits of the NIST-JANNAF Thermochemical Tables Fourth Edition*; Armstrong Flight Research Center, Edwards: Irvinem, CA, USA, 2021.